Pure Appl. Geophys.

https://doi.org/10.1007/s00024-023-03398-5

Pure and Applied Geophysics

Stress and Faulting Pattern in the Bam Region, SE Iran, Detected by Fault Instability Criterion and Fry Method

Ahad Nouri,[1] Behnam Rahimi,[1] Václav Vavryčuk,[2] and Hossein Sadeghi[1]

Abstract—In this study, we determine the stress release from the 2003 Bam earthquake (Mw 6.6) by applying the stress inversion technique to focal mechanisms of 199 aftershocks. There is no evidence of significant surface faulting that can be used to study the faulting pattern of the Bam fault zone. Therefore, we applied two independent methods for identifying the faulting pattern in this zone: the instability criterion based on the analysis of orientations of nodal planes of focal mechanisms with respect to the regional stress, and the Fry method based on the analysis of spatial clustering of aftershock foci. The results show that the fault associated with the 2003 Bam earthquake is well oriented for shearing under the present-day regional stress. We identified four sets of faults with a close angular relation to the maximum horizontal compression (SH_{max}) that have been (re)activated. These faults include strike-slip (right lateral and left lateral), thrust, and normal faults that are oriented approximately oblique, perpendicular, and parallel relative to the SH_{max}, respectively. The direction of the SH_{max} is N31° E. Based on the results, we propose to apply the instability criterion and the Fry method to seismic data as two valuable and independent techniques in order to constrain the kinematic and active faulting in the area.

Keywords: 2003 Bam earthquake, focal mechanism, stress inversion, Central-Eastern Iran.

1. Introduction

On December 26th, 2003 at 01:56:58 UTC the Mw 6.6 Bam earthquake with slip of up to 2 m (Jackson et al., 2006) occurred in the southeastern Iran, near the southern end of the Nyband–Gowk fault zone, on the SW side of the Lut block (Fig. 1) (Engdahl et al., 2006; Rahimi, 2012; Sadeghi et al., 2006; Shirzad & Moradi, 2022). The Global Centroid Moment Tensor (GCMT) center places the hypocenter of the earthquake at 58.24° E, 29.10° N with depth at ∼ 15 km. The fault plane solution reflects a right-lateral slip on a steeply eastward dipping fault, which had not previously been recognized.

Tectonic stress in the region is primarily influenced by convergence between the Arabian and Eurasian plates (Nouri et al., 2023). According to GPS measurements (Khorrami et al., 2019; Vernant et al., 2004), the convergence rate of these plates at a longitude of 51° E is ∼ 22 mm/year. It causes that this region is one of the most seismically active areas in the world (Ambraseys & Melville, 1982; Berberian, 1976, 2005). It seems that accommodating of deformation at different rates between the Central Iran and western Afghanistan is the main origin of the occurrence of large earthquakes along active faults in the Central and Eastern Iran (Jackson et al., 2006; Shirzad & Moradi, 2022). A comprehensive review of the historical seismicity of the region is given by Berberian (2005).

The evidence, as reviewed by Berberian (2005), Jackson et al. (2006), Khorrami et al. (2019), Vernant et al. (2004), and Walker and Jackson (2004), suggests that the tectonic activity of the region has been accommodated by a sub-parallel ∼ N–S right-lateral strike-slip fault system with a small component of thrusting, extending from the Central Iran to the western Afghanistan. This fault system is bounded by the left-lateral Doruneh fault and the Makran fold-and-thrust belt toward north and south, respectively.

Focal mechanisms of earthquakes are the main indicators of tectonic stress and processes in the Earth's crust. They also provide important information on the structure of a region. Hence, inverting for

[1] Department of Geology, Faculty of Science, Ferdowsi University of Mashhad, Azadi Sq., Mashhad, Khorasan Razavi, Iran. E-mail: ahad.nouri@mail.um.ac.ir

[2] Institute of Geophysics, Czech Academy of Sciences, Boční II/1401, 14100 Prague 4, Czech Republic.

Published online: 31 December 2023

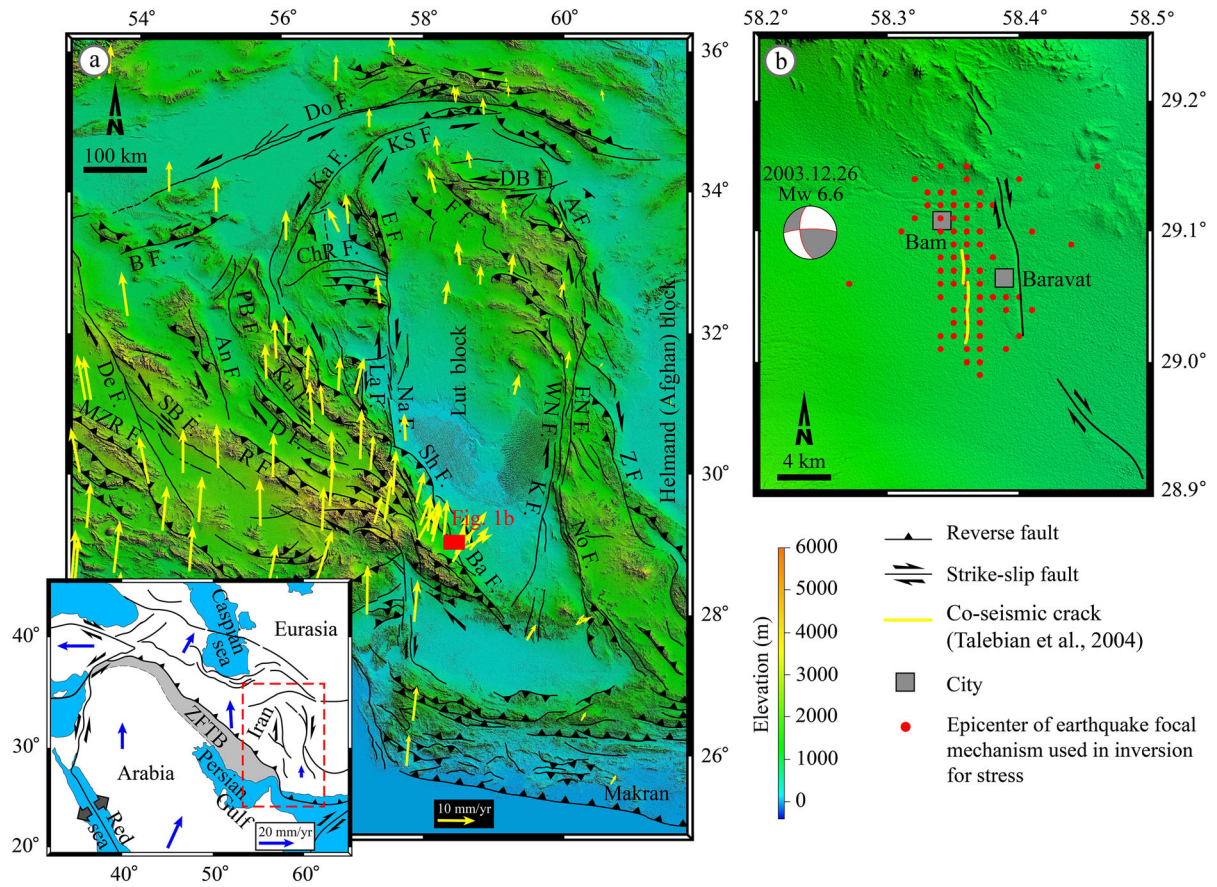

Fig. 1

a Fault map of the Central, Eastern, and Southern Iran (after Rashidi et al. (2019) and Sheikholeslami et al. (2021)). The GPS velocity vectors are from Khorrami et al. (2019) and Walpersdorf et al. (2014). *Do F.* Doruneh fault, *Ka F.* Kalmard fault, *B F* Biabanak fault, *KS F.* Kouh-e-Sarhangi fault, *DB F.* Dasht-e-Bayaz fault, *A F.* Abiz fault, *F F.* Ferdows fault, *E F.* Esfandiar fault, *ChR F.* Cheshmeh Rostam fault, *PB F.* Posht-e-Badam fault, *An F.* Anar fault, *De F.* Deh Shir fault, *MZR F.* Main Zagros Reverse fault, *SB F.* Shahr-e-Babak fault, *R F.* Rafsanjan fault, *D F.* Davaran fault, *Ku F.* Kuh-e-Baban fault, *La F.* Lakarkuh fault, *Na F.* Nayband fault, *Sh F.* Shahdad fault, *Ba F.* Bam fault, *EN F.* Eastern Neh fault, *WN F.* Western Neh fault, *Z F.* Zabol fault, *K F.* Kahurak fault, *No F.* Nosratabad fault. Inset indicates tectonic map of the Arabian-Eurasian collision zone (after Nouri et al. (2023) and references therein). GPS velocity vectors are from Reilinger et al. (2006). ZFTB: Zagros fold-and-thrust belt. **b** Fault map of the Bam area (Talebian et al., 2004; Tatar et al., 2005). The focal mechanism of the 2003 Bam earthquake is from the Global Centroid Moment Tensor catalogue. Note that the regular grid in epicenters shown in **b** is apparent, being caused by a limited location accuracy of analyzed aftershocks presented by Tatar et al., (2004, 2005)

the crustal stress from focal mechanisms is one of the main methods how to study the dynamics of the earth crust. As regards the seismic activity associated with the Bam earthquake, the main shock produced a series of enigmatic surface fractures that are small for such event (Mw 6.6) (Jackson et al., 2006). This makes it difficult to detect faulting pattern of this seismic fault zone from surface faulting like those that were detected for NW Iran (Faridi et al., 2017), for north of the Doruneh fault, NE Iran (Tadayon et al., 2017), for causing fault of the 2012 August 11 Varzaghan–Ahar earthquake (Mw 6.4, 6.2), NW Iran (Ghods et al., 2015) or for Dasht-e Bayaz fault zone, NE Iran (Tchalenko & Ambraseys, 1970). Many researchers have studied the 2003 Bam earthquake from a variety of viewpoints taking into account the rupture process, seismotectonics, earthquake hazard, active tectonics, and the velocity structure around the fault (Berberian, 2005; Jackson et al., 2006; Rahimi, 2012; Sadeghi et al., 2006; Shirzad & Moradi, 2022).

This paper aims to study tectonic stress in the region of the 2003 Bam earthquake and to provide a structural pattern of the Bam fault zone using the aftershock activity. Such study would facilitate better understanding active faulting processes, a long-term behavior of the active fault zone, and the seismic hazard of the area.

2. *Tectonic Setting*

Tectonics of Iran has a long and complex history associated with multistage evolution of the Tethys domain resulted from successive opening and closure of oceanic, back arc, and marginal basins (Berberian & King, 1981; Stern et al., 2021). Many researchers have been attempted to describe the shear movements in the Central-Eastern Iran because of significant implications for current deformation and the occurrence of several moderate to large earthquakes in the region (Berberian, 2014; Jackson et al., 2006; Meyer & Le Dortz, 2007; Tatar et al., 2004, 2005; Walker & Jackson, 2004; Walker et al., 2003; Walpersdorf et al., 2014). The driving stress associated with the convergence between the Arabian and Eurasian plates dominates the deformation through major structural elements in the Central-Eastern Iran. Historical (Ambraseys & Melville, 1982; Berberian, 2005) and instrumental (Engdahl et al., 2006) seismic studies in this region indicate several destructive earthquakes that caused even surface ruptures. The activated faults are mostly surrounding by relatively stable aseismic blocks with low rates of deformation. In the Central-Eastern Iran, the surface deformation is consistent with observations of fault plane solutions (Jackson et al., 2006; Khorrami et al., 2019; Vernant et al., 2004; Walker & Jackson, 2004).

The Central-Eastern Iran (Fig. 1) is characterized by an actively deforming strike-slip system, currently accommodating the ~ NE–SW Arabia–Eurasia convergence. Detailed GPS measurements in the Central-Eastern Iran (Khorrami et al., 2019) indicate an active deformation of 5.5–8.1 mm/year, decreasing toward the northern, eastern, and the southern boundaries of the region. The shear movements between the Central Iran and western Afghanistan are mostly taken up by NS right-lateral strike-slip faults. These faults are mainly extending along the eastern and western sides of the Lut block, whereas north of this fault system, shear takes place mostly along ~ EW-striking faults such as the Doruneh and Dasht-e Bayaz faults (Fig. 1) (Berberian, 1976, 2014; Khorrami et al., 2019; Vernant et al., 2004; Walker & Jackson, 2004; Walpersdorf et al., 2014). The strike-slip movements along the ~ NS-striking faults allow the Central-Eastern Iran to move NNE-ward by gradual indenting northward into the crust of NE Iran (Hollingsworth et al., 2010; Walker & Jackson, 2004; Walpersdorf et al., 2014). The ~ NS faults accommodates NS shortening by rotating counterclockwise of surrounded blocks around the vertical axis (Hollingsworth et al., 2010; Walker & Jackson, 2004; Walpersdorf et al., 2014). Further toward north of Iran, the convergence is mostly accommodated by ENE-SWS left-lateral shear along the Shahrud fault system, shortening in the Kopeh Dagh fold-and-thrust belt, and eventually ends as right-lateral movements along the NW–SE-striking Ashkabad fault zone (Hollingsworth et al., 2010; Khorrami et al., 2019; Vernant et al., 2004; Walker et al., 2021).

In this region, earthquakes take place in depth shallower than ~ 20 km (Engdahl et al., 2006) and sense of slip on faults is governed by the direction of the maximum compressional stress relative to strike of the active faults. Most of the seismogenic faults in the Central-Eastern Iran are known and their behavior is well understood (Berberian, 1976, 2014; Meyer & Le Dortz, 2007; Walker & Jackson, 2004; Walker et al., 2003, 2004). Generally, according to the studies in the Central-Eastern Iran, a dominant right-lateral slip occurs on ~ N-striking faults (e.g., Nayband fault), A left-lateral slip take places on the NE to ~ E-striking faults (e.g., Dorouneh and Dasht-e-Bayaz fauls), and a dominant reverse slip occurs on the NW-striking faults (e.g., Ferdows fault) (Fig. 1) (Berberian, 1976, 2014; Meyer & Le Dortz, 2007; Walker & Jackson, 2004; Walker et al., 2004).

3. Data and Method

3.1. Data

We compiled focal mechanisms of 199 aftershocks in the region, previously determined by Tatar et al., (2004, 2005), see Fig. 2. The aftershocks were monitored by an array of 23 portable three-component stations deployed in the epicentral area of the 2003 Bam earthquake and the focal mechanisms were determined using first-motion data. Focal mechanisms with a minimum of 12 P-wave polarities were selected for a further analysis and classified according to their quality into three categories (Tatar et al., 2004): category A (well constrained focal mechanisms with an error less than 20° for both two nodal planes), category B (focal mechanisms with an error less than 20° for one nodal plane), and category C (focal mechanisms with an error higher than 20°).

Also, we compiled locations of 1087 aftershocks ($1 < ML < 4.1$) associated with the 2003 Bam earthquake between December 2003 and March 2004 (Sadeghi et al., 2006; Tatar et al., 2005). These aftershocks were originally recorded and located using a 1-D velocity model (Tatar et al., 2005) and a 3-D velocity model (Sadeghi et al., 2006). Both epicentral and hypocentral uncertainties of the aftershock focal mechanisms are less than 1 km.

3.2. Method

First, we determined the tectonic stress by inverting the earthquake focal mechanisms. Then, we applied the Fry method to aftershock locations

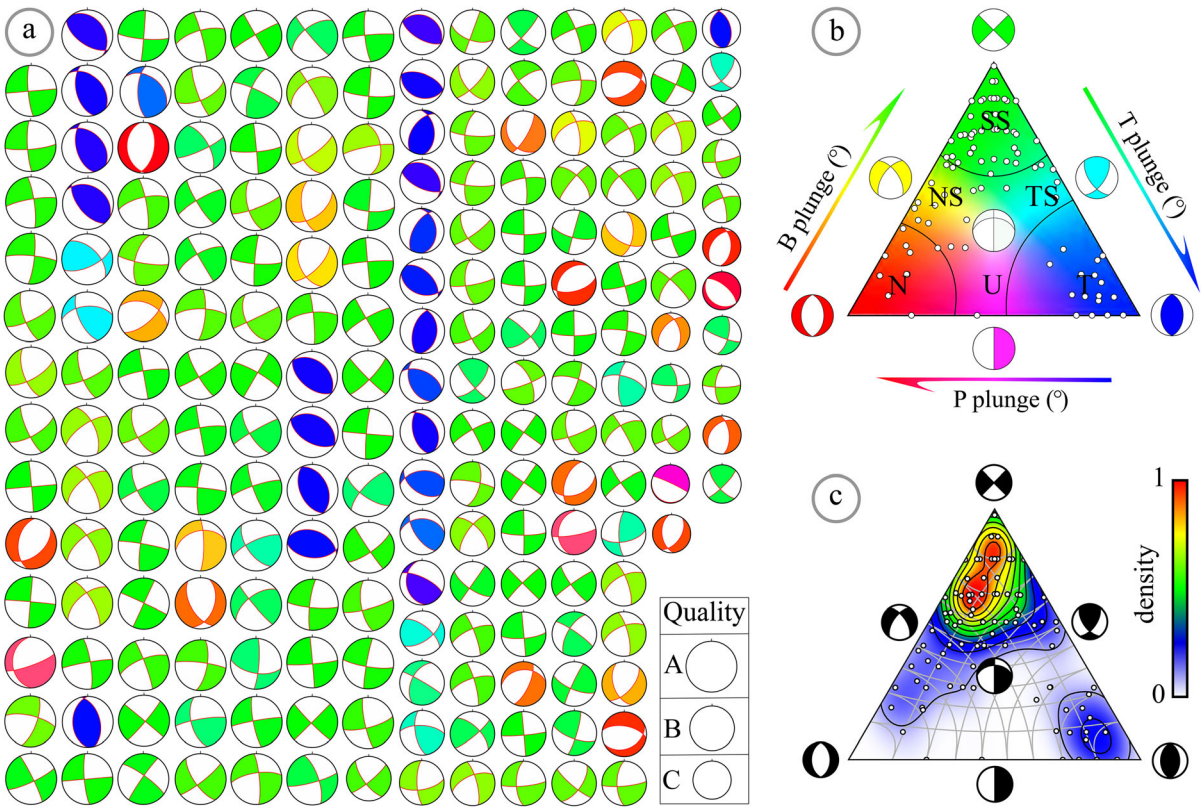

Fig. 2

a Focal mechanisms of 199 earthquakes used for determining the stress. Type of the mechanisms is colored based on the background color of the Frohlich's triangle diagram (Frohlich, 1992) presented in **b**. *SS* strike-sip faulting, *TS* thrust to strike-slip faulting, *T* thrust faulting, *NS* normal to strike-slip faulting, *N* normal faulting, and *U* unknown type of faulting. **c** Contoured Frohlich's triangle plots of all mechanisms used in this study

and the fault instability criterion to focal mechanisms in order to determine faulting pattern in the region.

3.2.1 Stress Inversion and the Fault Instability

To retrieve the principal stress directions and relative magnitude of principal stresses (i.e., the shape ratio) $R = (\sigma_1 - \sigma_2)/(\sigma_1 - \sigma_3)$, we invert the stress from focal mechanisms by using the iterative joint inversion proposed by Vavryčuk (2014). This method relies on the following three major assumptions: (1) slip on a fault plane occurs parallel to the direction of the maximum shear stress (Bott, 1959; Wallace, 1951), (2) all earthquakes on a fault have the same magnitudes of shear stress, and (3) stress is homogeneous and invariant in space and time.

A successful inversion for stress from focal mechanisms needs knowledge of which nodal plane is the fault. If such information is missing and faults are incorrectly interchanged with auxiliary planes, the stress inversion becomes inaccurate (Vavryčuk, 2014). This brings difficulty when inverting stress, because the ambiguity between two nodal planes of a mechanism should be resolved (Ouyed et al., 2022; Vavryčuk, 2015). To identify the true fault plane from the auxiliary one, usually some additional information such as geological data is required. Several researchers (Gephart & Forsyth, 1984; Lund & Slunga, 1999; Michael, 1987; Ouyed et al., 2022; Vavryčuk, 2014) pointed out that it is possible to distinguish most likely the true faults from the auxiliary planes using the joint inversion for stress and fault orientations. Lund and Slunga (1999) and Vavryčuk (2014) have proposed a method reducing the ambiguity problem by introducing the so-called fault instability criterion. In this method, the fault instability parameter I identifies the nodal plane that corresponds to the correct fault by:

1. applying the Mohr–Coulomb failure envelope to each nodal plane of a mechanism,
2. quantifying how close to the failure a nodal plane is,
3. selecting the most likely true faults by choosing a higher value of the fault instability (where $0 \leq I \leq 1$) that indicates a fault with an orientation nearest to an optimal orientation for shearing.

The fault instability I (Lund & Slunga, 1999; Vavryčuk, 2011, 2014) is defined as:

$$I = \frac{\tau - \mu(\sigma - 1)}{\mu + \sqrt{1 + \mu^2}}, \tag{1}$$

where τ, μ, and σ are the shear traction along a fault plane, the fault friction, and the effective normal traction, respectively.

In the joint stress inversion method, the stress is calculated in iterations and the iterative process continues until it reaches the highest instability I for selected nodal planes (Vavryčuk, 2014). The first iteration starts with randomly selected nodal planes as the faults, and the principal stress directions and the shape ratio R are calculated using the Michael's method (Michael, 1987). In the second iteration, the most likely true faults are identified by the fault instability criterion, and the stress inversion is run again with newly assigned fault planes. This process is repeated until the stress converges to some optimum value. In addition, the whole process is run for several values of friction to get the highest overall instability I. In addition to the four parameters of stress, this method determines two fault planes called the principal faults, which are characterized by the maximum instability ($I = 1$). These faults are optimally oriented for shearing under the given tectonic stress.

3.2.2 Fry Method

The orientation of active faults can alternatively be identified using spatial distribution of epicenters of earthquakes by applying the so-called Fry method. The method was introduced by Fry (1979) for finding the finite strain based on a two-dimensional analysis of nearest neighbors to a central reference point. This method plots translations, called the 'Fry' plots, of point objects by using each point as a central reference point for the translation. For N points, there are $N^2 - N$ translations. Vearncombe and Vearncombe (1999) employed the Fry method to study the 2D spatial distribution pattern of mineralization for identifying the trend(s) of mineralization. Here, we apply the Fry method on all aftershocks and on aftershocks declustered by the method proposed by Reasenberg (1985).

4. Results

The mechanisms of 199 aftershocks of the 2003 Bam earthquake used in the stress inversion show various types of faulting as shown in Fig. 2. The plunge of P, B, and T axes of mechanisms is fairly uniform and strike-slip faulting is the predominate mechanism (Fig. 2). The stress inversion of the focal mechanisms (Fig. 3a-d) yields a narrow distribution of the shape ratio and small confidence regions ($< 2.5°$) for the trend and plunge angles of the three principal stress axes. This refers to a reliable stress inversion and to a stable direction of the SH_{max}. A sub-vertical orientation is found for the intermediate principal stress, σ_2. The minimum and maximum principal stresses are found to be horizontal.

Fault planes selected by the stress inversion according to their instability I show the following strikes in relation to their sense of slip: (1) $\sim$ NNW–SSE-striking planes (mean strike: $345.2° \pm 8.3°$) showing a right-lateral sense of the slip (Fig. 3e), (2) $\sim$ ENE–WSW striking planes (mean strike: $345.2° \pm 8.3°$) characterized by a left-lateral sense of the slip (Fig. 3f), (3) NW–SE-striking planes (mean strike: $72.2° \pm 5.1°$) characterized by thrust faulting (Fig. 3g), and (4) NE–SW-striking planes (mean strike: $39.1° \pm 17.3°$) showing normal faulting (Fig. 3h).

The Fry plots of epicenters of all earthquakes show a $\sim$ N–S structural trend parallel to the co-seismic rupture (Fig. 4a). Applying the Fry plot to the epicenter locations of the declustered catalogue distinguishes four trends: N–S to NNW–SSE, approximately NE–SW, ENE–WSW, and SE to NW (Fig. 4b).

5. Discussion

5.1. Stress

5.1.1 Relation Between Results Stress Inversion and Active Faulting

The number of focal mechanisms used in the stress inversion is large enough for determining reliably the

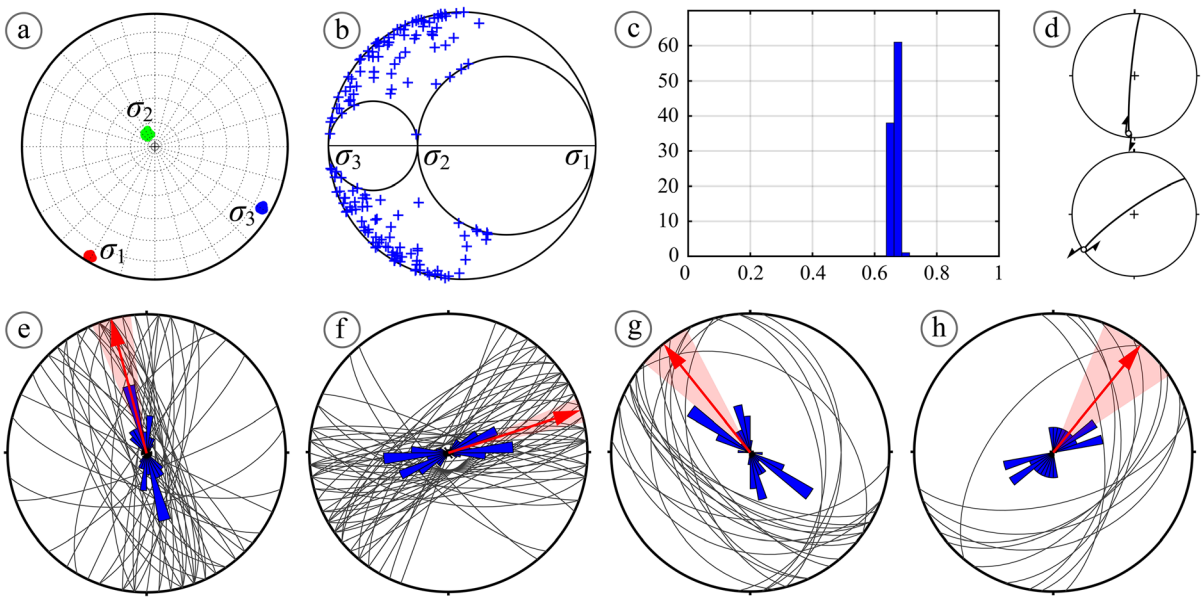

Fig. 3
Stress inversion results (**a**–**d**) and stereonet showing nodal planes selected by the stress inversion as fault planes (**e**–**h**). **a** Stereonet projections of the 95% confidence region for three principal stress axes σ_1, σ_2, and σ_3 indicated by red, green, and blue color, respectively, **b** Mohr circle diagram, **c** shape ratio histogram, **d** stereonet showing the two optimum (principal) faults, **e** right lateral faults, **f** left lateral faults, **g** thrust faults, **h** normal faults. Rose diagrams of strike of different fault types are illustrated in the background of the stereonets. The shadow red areas are the 95% confidence regions for the mean vector indicated by the red arrow

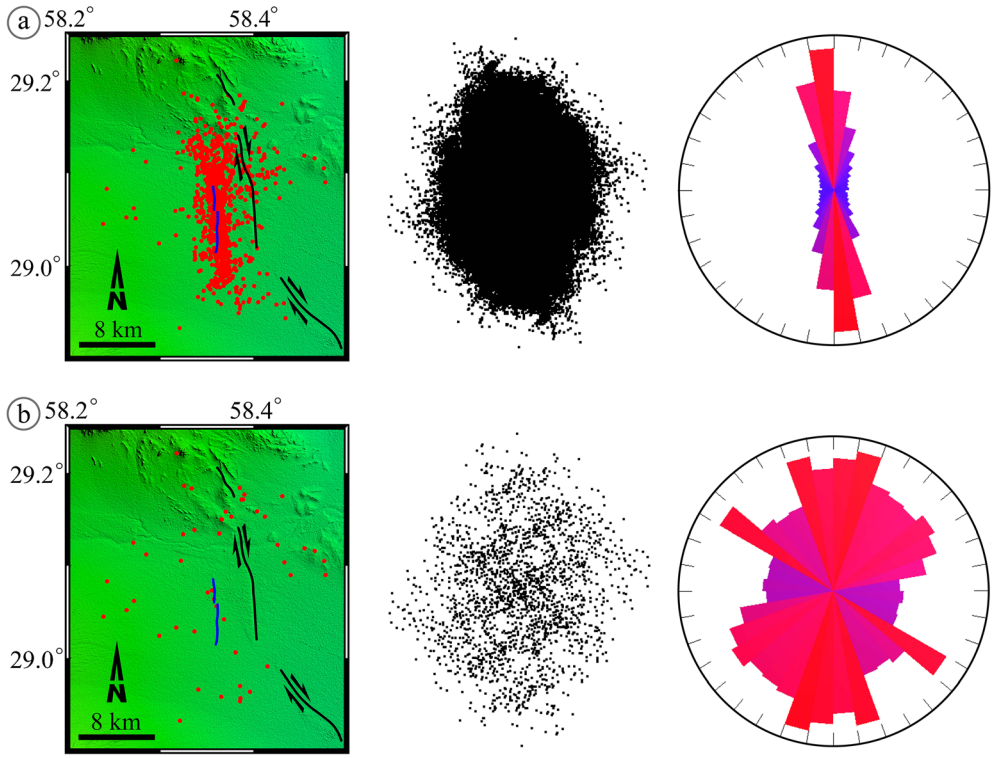

Fig. 4
Epicenters of all aftershocks (**a**) and of aftershocks from the declustered catalogue (**b**), along with their corresponding translations and rose diagrams depicting the trends of these translations (from left to right)

present-day local tectonic stress (Balfour et al., 2011; Michael et al., 1990). The value of the shape ratio R and plunge of σ_1, σ_2, and σ_3 axes point to a transpressional stress regime with a dominating strike-slip component (Simpson, 1997), as concluded by Walpersdorf et al. (2014). The shape ratio R is well-constrained with a small error, and the 95% confidence regions for the principal stresses are quite tight (Fig. 2 and Table 1). This implies that any interchangeability of σ_1, σ_2, and σ_3 would be difficult.

Applying the method of Lund and Townend (2007) to the stress inversion results, we found that the direction of the SH_{max} is N31° E. The direction of the surface trace of the Bam fault and co-seismic cracks of the 2003 Bam earthquake is ~ NS. Therefore, the angle between the SH_{max} and the fault trace is ~ 30°, which leads the fault to the right-lateral slip at an average rate of 2.1 ± 1.0 mm/year, and to the reverse slip at an average rate of ~ 0.3 ± 1.7 mm/year (Walpersdorf et al., 2014).

Table 1

The results of the stress inversion presented by the orientation of the principal stress axes σ_1, σ_2, and σ_3 given as trend/plunge in degree and the shape ratio R

N	σ_1 (°/°)	σ_2 (°/°)	σ_3 (°/°)	R	α (°)	S_{Hmax} (°)
199	211 ± 2.3/04	329 ± 2.5/81	120 ± 2.3/08	0.67	34.17	31

Direction of the maximum horizontal compression (S_{Hmax}) is in degree

N is the number of earthquake focal mechanisms used in the inversion for stress, α is the deviation angle (°)

The retrieved stress in the region is very similar to the regional stress determined by Sheikholeslami et al. (2021). Sheikholeslami et al. (2021) studied variations of stress in the Central Iran by inverting focal mechanisms of large earthquakes. In the region under our study, the σ_1 axis is approximately horizontal (Sheikholeslami et al., 2021) and is oriented oblique to structures highlighting the importance of the oblique-slip kinematics in the structural development of the region.

The results reveal that mostly one of the two optimally oriented faults, determined under the given stress field, activated during the 2003 Bam earthquake (strike/dip/rake: 185°/85°/173°). The second optimally oriented fault characterizing by a left-lateral slip (strike/dip/rake: 235°/81°/− 1°) was less active or was not activated at all during the 2003 Bam earthquake. The stress inversion results show that the ∼ N-striking Bam fault is in agreement with the NS-striking principal fault is optimally oriented for shearing (instability ≥ 0.9) under the retrieved active stress field (Figs. 1b and 2g). In addition, another SW-striking left-lateral fault is optimally oriented for shearing (Fig. 2g). The inversion results reveal that a system of ∼ NE–SW-striking faults with the left-lateral slip characterized by a high fault instability was picked in the final inversion for stress (Fig. 3b). This indicates that the NE-SW-striking faults are important for estimating potential seismic hazard in the region. However, the fault instability I identifies just how favorably oriented the fault is for shearing in the given stress field. Hence, the fault instability I does not show, whether the Mohr–Coulomb failure criterion is actually satisfied or not for this fault. Moreover, the fault instability I does not reflect the presence of fluids and the value of the pore pressure in the focal zone (Fojtíková & Vavryčuk, 2018; Vavryčuk et al., 2013).

5.1.2 *Homogeneity/Heterogeneity of Stress*

Michael (1991) discussed the issue of homogeneity/heterogeneity of stress according to the average misfit angle. The misfit angle is defined as the deviation between the observed and theoretically modelled slip direction on a fault plane. According to Michael (1991), when the average error of focal mechanisms is ∼ 20° and the average misfit angle is < 48°, the stress field is approximately homogeneous. Other researchers (e.g., Delvaux & Barth, 2010; Gephart & Forsyth, 1984) pointed out that nodal planes with the misfit angle > 30°–40° are too scattered, and hence such data have not been included into the inversion for stress. As shown in Fig. 5, a series of fault planes reaching high instability values shows a high misfit angle. This inconsistency between the fault instability and the misfit angle implies that other factors are needed to identify the homogeneity/heterogeneity of stress.

We propose six conditions for assigning the retrieved stress to be homogeneous: (1) 95% confidence regions of the σ_1 and σ_3 axes that do not overlap. (2) 95% confidence regions of the σ_1 and σ_2 axes with a high shape ratio (R) and/or those of the σ_2 and σ_3 axes with a low shape ratio and which do not overlap. (3) The well-constrained R value with a small error. (4) The well-constrained orientation of the SH_{max}. The orientation of the SH_{max} is stable and does not change when adding or rejecting focal mechanism(s) to the data set subjected to the inversion. (5) The retrieved stress regime should agree best with sense of most of the mechanisms. (6) The homogeneity of the structural pattern and/or absence of the structural variation. Since the structural pattern of a large-scale region is not homogenous, the focal mechanisms in such region cannot be inverted altogether in terms of the homogenous stress state. Hence, to study a regional variation in stress, the target region should be divided into sub-areas (Nouri et al., 2023). Based on the above considerations and as shown in Table 1 and

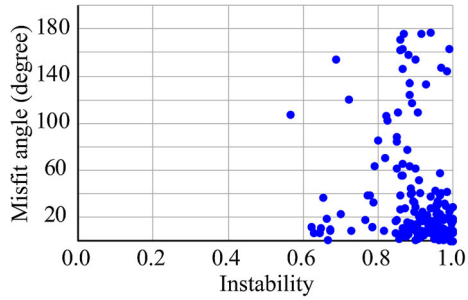

Fig. 5
Distribution of the misfit angle (°) versus instability I value in the scatter diagram

Fig. 2, we conclude that the stress in the region under study is very likely homogeneous.

5.2. Structural model

Different sets of fractures in the strike-slip system are widely studied by field studies (Coelho et al., 2006; Storti et al., 2006; Wilcox et al., 1973), analogue modelling (Coelho et al., 2006; Smith & Durney, 1992; Wilcox et al., 1973), and numerical modelling (Braun, 1994; McKinnon & de la Barra, 1998). From studies on sets of fractures, it is possible to estimate the angle between structural elements and the SH_{max} direction. At the time of failure, extensional and contractional structures are initiated parallel and perpendicular to the SH_{max}, respectively. Shear or conjugate sets of fractures develop oblique to the direction of the SH_{max}. The SH_{max} is approximately bisector of the acute angle of the conjugate fractures. These fractures are oriented approximately at $45° \pm \phi/2$ relative to the SH_{max}, where ϕ is the angle of internal friction of the rock and generally is equal to $\sim 30°$. However, precise angular relations of different sets of fractures in a volume of rock are dependent on fluid pressure, strain and stress rate and state, vorticity, and on the angle of internal friction (Coelho et al., 2006; Fossen, 2011).

The strikes of the fault planes selected from the nodal planes of focal mechanisms by the stress inversion show a broad variation. Some focal mechanisms show right-lateral slips on $\sim$ NE-SW-striking fault planes opposite to left-lateral slips on these fault planes. Also, some $\sim$ NW–SE-striking fault planes which are selected during the inversion for stress show left-lateral slips opposite to right-lateral slips on these fault planes. Such opposite sense of the slip on faults with the same strike was also reported by Aydin et al. (1992) after the 1989, Loma Prieta, California, earthquake, by Xu et al. (2020) after the 2019 Ridgecrest earthquake, and by Wetzler et al. (2021) along the Dead sea basin. It can result from: (1) the slip on pre-existing and weak faults that are not necessarily well-oriented relative to the current stress, and (2) small-scale stress perturbations due to mechanical anisotropy, interaction of faults, mainshock, and fluid pressure variations (Hardebeck & Okada, 2018; Plenefisch & Bonjer, 1997; Stein, 1999; Zoback, 1992; Zoback et al., 1987).

The structural trend identified in the Fry plot agrees well with the co-seismic crack, the strike of the Bam fault, and the instability-based selected nodal planes as the faults (Figs. 3, 4). Based on the results of the stress inversion, the above description, and knowing that active tectonic studies are mostly constrained by earthquake focal mechanisms (Heidbach et al., 2018; Vavryčuk & Adamová, 2018; Zoback, 1992), we propose a kinematic model to illustrate the main features of the active faulting in the Bam area, as shown in Fig. 6.

Such model is proposed for north of the Doruneh fault, NE Iran, by Tadayon et al. (2017), according to geological data, and for north of China by Li et al. (2015) according to the seismic data. The 2003 Bam earthquake occurred on a blind fault (Jackson et al., 2006; Tatar et al., 2005). The $\sim$ N-striking right-lateral fault (Fig. 6) is concluded by Talebian et al. (2004), Tatar et al. (2005), and Sadeghi et al. (2006). The principle slip on the fault at depth has occurred in south of the fault zone (Talebian et al., 2004). Tatar et al. (2005) and Jackson et al. (2006) believed that

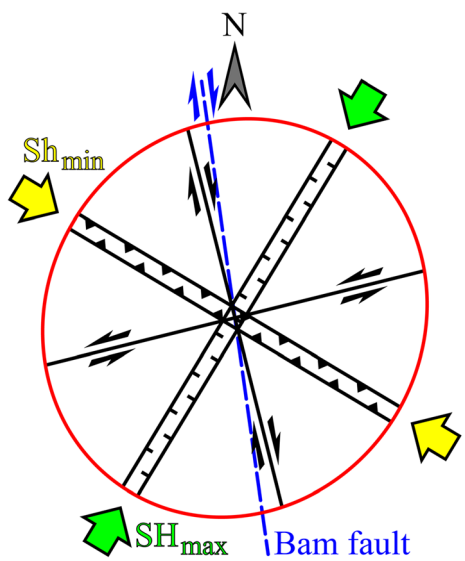

Fig. 6
Simplified diagram illustrating the fault pattern of the Bam fault zone deduced from seismic data. The faults parallel to the maximum and minimum horizontal compression stress are the normal and thrust faults, respectively, and others are shear (strike-slip) faults. Diameters of the stress ellipsoid as shown in red color are based on the stress ratio

the fault has been propagated northward. According to the Frohlich's diagram (Frohlich, 1992) (Fig. 2), mechanisms of the aftershocks mainly show strike-slip faulting. Nevertheless, thrust faulting is also considerable. According to Jackson et al. (2006), in addition to the right-lateral movements, a reverse component of the slip was detected along the Bam-Baravat escarpment revealed in the radar interferograms and field studies. This implies that faulting may be in the early stages of a slip partitioning of the oblique convergence across the region into the strike-slip and reverse components (Jackson et al., 2006).

The results allow us to suggest that the instability criterion proposed by Lund and Slunga (1999) and Vavryčuk (2011, 2014) selects the fault planes with the best agreement with seismic and geological evidences. Besides, the Fry plot technique proposed by Vearncombe and Vearncombe (1999) can be utilized to identify the structural trends from seismic data.

6. Conclusion

The 2003 Bam earthquake (Mw 6.6) aftershock sequence occurred along a relatively unknown fault zone. The results of the analysis of the fault instability criterion and the Fry method consistently show that the aftershocks of the 2003 Bam earthquake were distributed along faults and subfaults well oriented for shearing under the present-day regional stress. This allows us to propose that the Fry plot method, previously used to determine the mineralization trends, can also serve as a novel supporting technique for structural analysis utilizing seismic data.

Acknowledgements

We thank Editor and two anonymous reviewers for their constructive and helpful reviews. We thank Dr. M. Tatar for kindly providing the aftershock data of 2003 Bam earthquake and his helpful comments and suggestions. The work was partly supported by the Czech Science Foundation, grant No. 22-10747S.

Author contributions Ahad Nouri: Conception and design of study, Data collection, Software, Interpretation, Writing/drafting/editing.Behnam Rahimi: Conception and design of study, Interpretation, Reading/editing the manuscript. Václav Vavryčuk: Interpretation, Reading/editing the manuscript.Hossein Sadeghi: Acquisition of a part of data, Reading/editing the manuscript.

Funding

The authors declare that no funds, or other support were received during the preparation of this manuscript.

Data and codes availability

Plotting of the focal mechanism of earthquakes on the Frohlich's diagram was performed by Orient software developed by Vollmer (2015) (https://www.frederickvollmer.com/orient/index.html). The Fry method (Fry, 1979) was performed by SpaDIS software developed by Vearncombe and Vearncombe (1999) (https://www.sjsresource.com.au). The inversion for stress was performed with open-public Matlab code STRESSINVERSE (https://www.ig.cas.cz/stress-inverse).

Declarations

Conflict of interest The authors declare that they have no known competing financial or non-financial interests or personal relationships that could have appeared to influence the work reported in this paper.

Publisher's Note Springer Nature remains neutral with regard to jurisdictional claims in published maps and institutional affiliations.

References

Ambraseys, N. N., & Melville, C. P. (1982). *A history of Persian earthquakes* (p. 219). Cambridge University Press.

Aydin, A., Johnson, A. M., & Fleming, R. W. (1992). Right-lateral-reverse surface rupture along the San Andreas and Sargent faults associated with the October 17, 1989, Loma Prieta, California, earthquake. *Geology, 20*, 1063–1067. https://doi.org/10.1130/0091-7613(1992)020%3c1063:rlrsra%3e2.3.co;2

Balfour, N., Cassidy, J., Dosso, S., & Mazzotti, S. (2011). Mapping crustal stress and strain in southwest British Columbia. *Journal of Geophysical Research: Solid Earth*. https://doi.org/10.1029/2010jb008003

Berberian, M. (1976). Documented earthquake faults in Iran. *Geological Survey of Iran, 39*, 143–186.

Berberian, M. (2005). The 2003 Bam urban earthquake: A predictable seismotectonic pattern along the western margin of the rigid Lut block, southeast Iran. *Earthquake Spectra, 21*, 35–99. https://doi.org/10.1193/1.2127909

Berberian, M. (2014). *Earthquakes and coseismic surface faulting on the Iranian Plateau*. Elsevier.

Berberian, M., & King, G. (1981). Towards a paleogeography and tectonic evolution of Iran. *Canadian Journal of Earth Sciences, 18*, 210–265. https://doi.org/10.1139/e81-019

Bott, M. H. P. (1959). The mechanics of oblique slip faulting. *Geological Magazine, 96*, 109–117. https://doi.org/10.1017/s0016756800059987

Braun, J. (1994). Three-dimensional numerical simulations of crustal-scale wrenching using a non-linear failure criterion. *Journal of Structural Geology, 16*, 1173–1186. https://doi.org/10.1016/0191-8141(94)90060-4

Coelho, S., Passchier, C., & Marques, F. (2006). Riedel-shear control on the development of pennant veins: Field example and analogue modelling. *Journal of Structural Geology, 28*, 1658–1669. https://doi.org/10.1016/j.jsg.2006.05.009

Delvaux, D., & Barth, A. (2010). African stress pattern from formal inversion of focal mechanism data. *Tectonophysics, 482*, 105–128. https://doi.org/10.1016/j.tecto.2009.05.009

Engdahl, E. R., Jackson, J. A., Myers, S. C., Bergman, E. A., & Priestley, K. (2006). Relocation and assessment of seismicity in the Iran region. *Geophysical Journal International, 167*, 761–778. https://doi.org/10.1111/j.1365-246x.2006.03127.x

Faridi, M., Burg, J.-P., Nazari, H., Talebian, M., & Ghorashi, M. (2017). Active faults pattern and interplay in the Azerbaijan region (NW Iran). *Geotectonics, 51*, 428–437.

Fojtíková, L., & Vavryčuk, V. (2018). Tectonic stress regime in the 2003–2004 and 2012–2015 earthquake swarms in the Ubaye Valley, French Alps. *Pure and Applied Geophysics, 175*, 1997–2008. https://doi.org/10.1007/s00024-018-1792-2

Fossen, H. (2011). *Structural geology*. Cambridge University Press.

Frohlich, C. (1992). Triangle diagrams: Ternary graphs to display similarity and diversity of earthquake focal mechanisms. *Physics of the Earth and Planetary Interiors, 75*, 193–198. https://doi.org/10.1016/0031-9201(92)90130-n

Fry, N. (1979). Random point distributions and strain measurement in rocks. *Tectonophysics, 60*, 89–105. https://doi.org/10.1016/0040-1951(79)90135-5

Gephart, J. W., & Forsyth, D. W. (1984). An improved method for determining the regional stress tensor using earthquake focal mechanism data: Application to the San Fernando earthquake sequence. *Journal of Geophysical Research: Solid Earth, 89*, 9305–9320. https://doi.org/10.1029/jb089ib11p09305

Ghods, A., Shabanian, E., Bergman, E., Faridi, M., Donner, S., Mortezanejad, G., & Aziz-Zanjani, A. (2015). The Varzaghan-Ahar, Iran, Earthquake Doublet (M w 6.4, 6.2): Implications for the geodynamics of northwest Iran. *Geophysical Journal International, 203*, 522–540. https://doi.org/10.1093/gji/ggv306

Hardebeck, J. L., & Okada, T. (2018). Temporal stress changes caused by earthquakes: A review. *Journal of Geophysical Research: Solid Earth, 123*, 1350–1365. https://doi.org/10.1002/2017jb014617

Heidbach, O., Rajabi, M., Cui, X., Fuchs, K., Müller, B., Reinecker, J., Reiter, K., Tingay, M., Wenzel, F., & Xie, F. (2018). The World Stress Map database release 2016: Crustal stress pattern across scales. *Tectonophysics, 744*, 484–498. https://doi.org/10.1016/j.tecto.2018.07.007

Hollingsworth, J., Fattahi, M., Walker, R., Talebian, M., Bahroudi, A., Bolourchi, M. J., Jackson, J., & Copley, A. (2010). Oroclinal bending, distributed thrust and strike-slip faulting, and the accommodation of Arabia-Eurasia convergence in NE Iran since the Oligocene. *Geophysical Journal International, 181*, 1214–1246. https://doi.org/10.1111/j.1365-246x.2010.04591.x

Jackson, J., Bouchon, M., Fielding, E., Funning, G., Ghorashi, M., Hatzfeld, D., Nazari, H., Parsons, B., Priestley, K., & Talebian, M. (2006). Seismotectonic, rupture process, and earthquake-hazard aspects of the 2003 December 26 Bam, Iran, earthquake. *Geophysical Journal International, 166*, 1270–1292. https://doi.org/10.1111/j.1365-246x.2006.03056.x

Khorrami, F., Vernant, P., Masson, F., Nilfouroushan, F., Mousavi, Z., Nankali, H., Saadat, S. A., Walpersdorf, A., Hosseini, S., & Tavakoli, P. (2019). An up-to-date crustal deformation map of Iran using integrated campaign-mode and permanent GPS velocities. *Geophysical Journal International, 217*, 832–843. https://doi.org/10.1093/gji/ggz045

Li, B., Atakan, K., Sørensen, M. B., & Havskov, J. (2015). Stress pattern of the Shanxi rift system, North China, inferred from the inversion of new focal mechanisms. *Geophysical Journal International, 201*, 505–527. https://doi.org/10.1093/gji/ggv025

Lund, B., & Slunga, R. (1999). Stress tensor inversion using detailed microearthquake information and stability constraints: Application to Ölfus in southwest Iceland. *Journal of Geophysical Research: Solid Earth, 104*, 14947–14964. https://doi.org/10.1029/1999jb900111

Lund, B., & Townend, J. (2007). Calculating horizontal stress orientations with full or partial knowledge of the tectonic stress tensor. *Geophysical Journal International, 170*, 1328–1335. https://doi.org/10.1111/j.1365-246x.2007.03468.x

McKinnon, S. D., & de la Barra, I. G. (1998). Fracture initiation, growth and effect on stress field: A numerical investigation. *Journal of Structural Geology, 20*, 1673–1689. https://doi.org/10.1016/s0191-8141(98)00080-7

Meyer, B., & Le Dortz, K. (2007). Strike-slip kinematics in central and eastern Iran: Estimating fault slip-rates averaged over the Holocene. *Tectonics*. https://doi.org/10.1029/2006tc002073

Michael, A. J. (1987). Use of focal mechanisms to determine stress: A control study. *Journal of Geophysical Research: Solid Earth, 92*, 357–368. https://doi.org/10.1029/jb092ib01p00357

Michael, A. J. (1991). Spatial variations in stress within the 1987 Whittier Narrows, California, aftershock sequence: New techniques and results. *Journal of Geophysical Research: Solid Earth, 96*, 6303–6319. https://doi.org/10.1029/91jb00195

Michael, A. J., Ellsworth, W. L., & Oppenheimer, D. H. (1990). Coseismic stress changes induced by the 1989 Loma Prieta, California earthquake. *Geophysical Research Letters, 17*, 1441–1444. https://doi.org/10.1029/gl017i009p01441

Nouri, A., Rahimi, B., Vavryčuk, V., & Ghaemi, F. (2023). Spatially varying crustal stress along the Zagros seismic belt inferred from earthquake focal mechanisms. *Tectonophysics, 846*, 229653. https://doi.org/10.1016/j.tecto.2022.229653

Ouyed, R., Boughacha, M. S., Bezzeghoud, M., & Vavryčuk, V. (2022). Fault plane picking from focal mechanisms in reverse faulting stress: Application to the Mw6.9 Boumerdes (Algeria) earthquake sequence. *Journal of African Earth Sciences, 196*, 104729. https://doi.org/10.1016/j.jafrearsci.2022.104729

Plenefisch, T., & Bonjer, K.-P. (1997). The stress field in the Rhine Graben area inferred from earthquake focal mechanisms and estimation of frictional parameters. *Tectonophysics, 275*, 71–97. https://doi.org/10.1016/s0040-1951(97)00016-4

Rahimi, B. (2012). Spatial analysis of the frequency–magnitude distribution of aftershock activity of 2003 Bam earthquake: Southeast Iran. *International Journal of Earth Sciences, 101*, 1441–1450. https://doi.org/10.1007/s00531-011-0716-5

Rashidi, A., Khatib, M. M., Nilfouroushan, F., Derakhshani, R., Mousavi, S. M., Kianimehr, H., & Djamour, Y. (2019). Strain rate and stress fields in the West and South Lut block, Iran: Insights from the inversion of focal mechanism and geodetic data. *Tectonophysics, 766*, 94–114. https://doi.org/10.1016/j.tecto.2019.05.020

Reasenberg, P. (1985). Second-order moment of central California seismicity, 1969–1982. *Journal of Geophysical Research: Solid Earth, 90*, 5479–5495. https://doi.org/10.1029/jb090ib07p05479

Reilinger, R., McClusky, S., Vernant, P., Lawrence, S., Ergintav, S., Cakmak, R., Ozener, H., Kadirov, F., Guliev, I., & Stepanyan, R. (2006). GPS constraints on continental deformation in the Africa-Arabia-Eurasia continental collision zone and implications for the dynamics of plate interactions. *Journal of Geophysical Research: Solid Earth*. https://doi.org/10.1029/2005jb004051

Sadeghi, H., Aghda, S. F., Suzuki, S., & Nakamura, T. (2006). 3-D velocity structure of the 2003 Bam earthquake area (SE Iran): Existence of a low-Poisson's ratio layer and its relation to heavy damage. *Tectonophysics, 417*, 269–283. https://doi.org/10.1016/j.tecto.2006.01.005

Sheikholeslami, M. R., Mobayen, P., Javadi, H. R., & Ghassemi, M. R. (2021). Stress field and tectonic regime of Central Iran from inversion of the earthquake focal mechanisms. *Tectonophysics, 813*, 228931. https://doi.org/10.1016/j.tecto.2021.228931

Shirzad, T., & Moradi, A. (2022). Analysis of the shallow crustal structure of the Bam Fault Zone, Iran, using the surface wave and first-arrival P-wave tomography approaches. *Physics of the Earth and Planetary Interiors, 324*, 106852. https://doi.org/10.1016/j.pepi.2022.106852

Simpson, R. W. (1997). Quantifying Anderson's fault types. *Journal of Geophysical Research: Solid Earth, 102*, 17909–17919. https://doi.org/10.1029/97jb01274

Smith, J., & Durney, D. (1992). Experimental formation of brittle structural assemblages in oblique divergence. *Tectonophysics, 216*, 235–253. https://doi.org/10.1016/0040-1951(92)90399-q

Stein, R. S. (1999). The role of stress transfer in earthquake occurrence. *Nature, 402*, 605–609.

Stern, R. J., Moghadam, H. S., Pirouz, M., & Mooney, W. (2021). The geodynamic evolution of Iran. *Annual Review of Earth and Planetary Sciences, 49*, 9–36. https://doi.org/10.1146/annurev-earth-071620-052109

Storti, F., Rossetti, F., Läufer, A. L., & Salvini, F. (2006). Consistent kinematic architecture in the damage zones of intraplate strike-slip fault systems in North Victoria Land, Antarctica and implications for fault zone evolution. *Journal of Structural Geology, 28*, 50–63. https://doi.org/10.1016/j.jsg.2005.09.004

Tadayon, M., Rossetti, F., Zattin, M., Nozaem, R., Calzolari, G., Madanipour, S., & Salvini, F. (2017). The post-Eocene evolution of the Doruneh fault region (Central Iran): The intraplate response to the reorganization of the Arabia-Eurasia collision zone. *Tectonics, 36*, 3038–3064. https://doi.org/10.1002/2017tc004595

Talebian, M., Fielding, E. J., Funning, G. J., Ghorashi, M., Jackson, J., Nazari, H., Parsons, B., Priestley, K., Rosen, P. A., & Walker, R. (2004). The 2003 Bam (Iran) earthquake: Rupture of a blind strike-slip fault. *Geophysical Research Letters*. https://doi.org/10.1029/2004gl020058

Tatar, M., Hatzfeld, D., Moradi, A., & Paul, A. (2005). The 2003 December 26 Bam earthquake (Iran), Mw 6.6, aftershock sequence. *Geophysical Journal International, 163*, 90–105. https://doi.org/10.1111/j.1365-246x.2005.02639.x

Tatar, M., Hatzfeld, D., Moradi, A., Paul, A., Farahbod, A., & Mokhtari, M. (2004). Aftershocks study of the 26 December 2003 Bam earthquake. *JSEE, 5*, 23–31.

Tchalenko, J., & Ambraseys, N. N. (1970). Structural analysis of the Dasht-e Bayaz (Iran) earthquake fractures. *Geological Society of America Bulletin, 81*, 41–60. https://doi.org/10.1130/0016-7606(1970)81[41:saotdb]2.0.co;2

Vavryčuk, V. (2011). Principal earthquakes: Theory and observations from the 2008 West Bohemia swarm. *Earth and Planetary Science Letters, 305*, 290–296. https://doi.org/10.1016/j.epsl.2011.03.002

Vavryčuk, V. (2014). Iterative joint inversion for stress and fault orientations from focal mechanisms. *Geophysical Journal International, 199*, 69–77. https://doi.org/10.1093/gji/ggu224

Vavryčuk, V. (2015). Earthquake mechanisms and stress field. In M. Beer, I. Kougioumtzoglou, E. Patelli, & I. Au (Eds.), *Encyclopedia of earthquake engineering* (pp. 728–746). Springer. https://doi.org/10.1007/978-3-642-35344-4_295

Vavryčuk, V., & Adamová, P. (2018). Detection of stress anomaly produced by interaction of compressive fault steps in the West Bohemia swarm region, Czech Republic. *Tectonics, 37*, 4212–4225. https://doi.org/10.1111/j.1365-246x.2011.05122.x

Vavryčuk, V., Bouchaala, F., & Fischer, T. (2013). High-resolution fault image from accurate locations and focal mechanisms of the 2008 swarm earthquakes in West Bohemia, Czech Republic. *Tectonophysics, 590*, 189–195. https://doi.org/10.1016/j.tecto.2013.01.025

Vearncombe, J., & Vearncombe, S. (1999). The spatial distribution of mineralization; applications of Fry analysis. *Economic Geology, 94*, 475–486. https://doi.org/10.2113/gsecongeo.94.4.475

Vernant, P., Nilforoushan, F., Hatzfeld, D., Abbassi, M., Vigny, C., Masson, F., Nankali, H., Martinod, J., Ashtiani, A., & Bayer, R. (2004). Present-day crustal deformation and plate kinematics in the Middle East constrained by GPS measurements in Iran and northern Oman. *Geophysical Journal International, 157*, 381–398. https://doi.org/10.1111/j.1365-246x.2004.02222.x

Vollmer, F. W. (2015). Orient 3: a new integrated software program for orientation data analysis, kinematic analysis, spherical projections, and Schmidt plots. *Geological Society of America Abstracts with Programs*, *47*(7), 49.

Walker, R., Bezmenov, Y., Begenjev, G., Carolin, S., Dodds, N., Gruetzner, C., Jackson, J., Mirzin, R., Mousavi, Z., & Rhodes, E. (2021). Slip-rate on the Main Köpetdag (Kopeh Dagh) strike-slip fault, Turkmenistan, and the active tectonics of the South Caspian. *Tectonics, 40*, e2021TC006846. https://doi.org/10.1029/2021tc006846

Walker, R., & Jackson, J. (2004). Active tectonics and late Cenozoic strain distribution in central and eastern Iran. *Tectonics*. https://doi.org/10.1029/2003tc001529

Walker, R., Jackson, J., & Baker, C. (2003). Surface expression of thrust faulting in eastern Iran: Source parameters and surface deformation of the 1978 Tabas and 1968 Ferdows earthquake sequences. *Geophysical Journal International, 152*, 749–765. https://doi.org/10.1046/j.1365-246x.2003.01886.x

Walker, R., Jackson, J., & Baker, C. (2004). Active faulting and seismicity of the Dasht-e-Bayaz region, eastern Iran. *Geophysical Journal International, 157*, 265–282. https://doi.org/10.1111/j.1365-2966.2004.02179.x

Wallace, R. E. (1951). Geometry of shearing stress and relation to faulting. *The Journal of Geology, 59*, 118–130. https://doi.org/10.1086/625831

Walpersdorf, A., Manighetti, I., Mousavi, Z., Tavakoli, F., Vergnolle, M., Jadidi, A., Hatzfeld, D., Aghamohammadi, A., Bigot, A., & Djamour, Y. (2014). Present-day kinematics and fault slip rates in eastern Iran, derived from 11 years of GPS data. *Journal of Geophysical Research: Solid Earth, 119*, 1359–1383. https://doi.org/10.1002/2013jb010620

Wetzler, N., Sagy, A., Marco, S., & Reches, Z. E. (2021). Asymmetry of faults and stress patterns within the Dead Sea basin as displayed by seismological analysis. *Tectonophysics, 819*, 229069. https://doi.org/10.1016/j.tecto.2021.229069

Wilcox, R. E., Harding, T. T., & Seely, D. (1973). Basic wrench tectonics. *Aapg Bulletin, 57*, 74–96. https://doi.org/10.1306/819a424a-16c5-11d7-8645000102c1865d

Xu, X., Sandwell, D. T., Ward, L. A., Milliner, C. W., Smith-Konter, B. R., Fang, P., & Bock, Y. (2020). Surface deformation associated with fractures near the 2019 Ridgecrest earthquake sequence. *Science, 370*, 605–608. https://doi.org/10.1126/science.abd1690

Zoback, M. L. (1992). First-and second-order patterns of stress in the lithosphere: The World Stress Map Project. *Journal of Geophysical Research: Solid Earth, 97*, 11703–11728. https://doi.org/10.1029/92jb00132

Zoback, M. D., Zoback, M. L., Mount, V. S., Suppe, J., Eaton, J. P., Healy, J. H., Oppenheimer, D., Reasenberg, P., Jones, L., & Raleigh, C. B. (1987). New evidence on the state of stress of the San Andreas fault system. *Science, 238*, 1105–1111. https://doi.org/10.1126/science.238.4830.1105

(Received September 17, 2023, revised November 20, 2023, accepted November 27, 2023)